Hysteretic Performance of Angle Steel Connections in a Timber-Concrete Composite System

Lan Xie,[a] Guojing He,[b,*] Xiaodong (Alice) Wang,[c] Xiao Tang,[d] and Roberto Crocetti [e]

Timber–concrete composite systems are widely used in Europe, North America, and Australasia, primarily due to their good mechanical performance in terms of statics, dynamics, and seismic response. In addition, the concrete slab provides excellent protection to the timber, making such systems suitable for outdoor application. The seismic performance of timber–concrete composites is normally governed by their ductility and energy dissipation capacity. However, few design codes address the ductility and energy dissipation capacity of timber–concrete composite systems, owing to a lack of reliable performance data. Therefore, further research on the hysteretic performance of timber–concrete composite systems is necessary. In this study, six timber–concrete composite specimens with an angle steel connection of the same size were investigated using reversed cyclic tests. The corresponding failure modes were observed, and the salient features of the connection, *i.e.*, the stiffness, ductility, and energy dissipation, were computed from the test results. The force mechanism of the timber–concrete composite specimens under reversed cyclic load was analyzed. Equations were presented to calculate the yield force and negative force in the same load step. A comparison of the test results and the theoretical results indicated good agreement.

DOI: 10.15376/biores.17.1.1270-1284

Keywords: Timber–concrete composite structure; TCC; Hysteretic performance; Energy dissipation capacity; Ductility

*Contact information: a: College of Civil Engineering, Changsha University, 98 Hongshan Road, Changsha, Hunan 410022 China; b: Department of Civil Engineering and Mechanics, Central South University of Forestry and Technology, 498 Shaoshan Road, Changsha, Hunan 410004 China; c: Department of Wood and Forest Sciences, Laval University, Quebec G1V 0A6 Canada; d: Changsha Urban Construction Secondary Vocational School, Nongyuan Rd, Changsha, Hunan 410126 China; e: Department of Civil and Architectural Engineering, KTH Royal Institute of Technology, Stockholm 10044 Sweden; *Corresponding authors: lily.csuft.xie@gmail.com; xieyuantaixielan@126.com*

INTRODUCTION

Timber–concrete composite (TCC) systems are a type of composite system in which a timber member and a concrete slab are connected to exhibit composite behavior. Timber–concrete composite systems have been widely used in Europe, North America, South America, and Australasia for new buildings and new bridges as well as for upgrading existing timber floors (Calil and Monlina 2008; Yeoh *et al*. 2011; Molina *et al*. 2019; Wacker *et al*. 2020). This is due to their good mechanical performance in terms of statics, dynamics, and seismic response (Rijal *et al.* 2015), as well as their environmental friendliness (Rodrigues *et al*. 2013), acoustics (Martins *et al*. 2015), and fire-resistant properties (Frangi *et al*. 2009; Frangi *et al*. 2010; Skinner *et al.* 2014).

Although the static characteristics of TCC systems have been thoroughly investigated (Lamothe *et al*. 2020; Zhang *et al*. 2021), their influence on seismic performance is not clearly understood. The seismic performance of TCC systems is normally governed by its structural ductility (He *et al*. 2020). Thus, the measurement of its hysteretic characteristics, *e.g.*, ductility and energy dissipation capacity, is necessary to investigate the seismic performance of TCC systems.

In a timber–concrete hybrid system, the hysteretic curve exhibits strength and stiffness degradation as well as a pinching effect (Isoda and Tesfamariam 2016; Kawai *et al.* 2016). Isoda and Tesfamariam (2016) found that the connection system has considerable influence on the hysteretic behaviour of a timber–concrete hybrid system. Similarly, Leijten *et al*. (2006) found that the deformation and energy dissipation of the timber frame structure depends on the nonlinear deformation of the connector. Thus, the connectors in the TCC system play a vital role in the shear capacity, seismic performance, and resistance to vertical uplift between the upper concrete slab and the bottom timber beam (Zhu *et al*. 2019). The shear strength, stiffness, and stress mechanisms of connectors have been investigated (Mascia and Soriano 2004; Dias *et al*. 2010; He *et al*. 2016; Xie *et al*. 2017). While the seismic performance of the connections in timber and hybrid systems have been studied (Izzi and Polastri 2019; Yang *et al.* 2020), only a few studies have addressed the hysteresis of the connections in TCC systems (Carrero *et al.* 2020). In addition, no research or code is available to guide the seismic design of TCC systems.

A TCC system with angle steel connection performs well under static loads (Chen 2016). However, its hysteresis property has not been thoroughly investigated. To investigate the hysteretic behaviour of angle steel connectors in a TCC system, six identical specimens were manufactured and subjected to reverse cyclic displacement testing. The failure modes were observed, and the characteristics of each connection, *i.e.*, the stiffness, ductility, and energy dissipation, were computed from the experimental results. In addition, the force mechanism of the TCC specimens under a reverse cyclic load was analyzed. The research will be referable for the seismic design for the TCC systems.

EXPERIMENTAL

Design and Fabrication of the Reversed Cyclic Specimens

Tests were conducted on six TCC specimens of the same size with an angle steel connection. Each specimen had three components: a timber block, concrete blocks, and shear connectors.

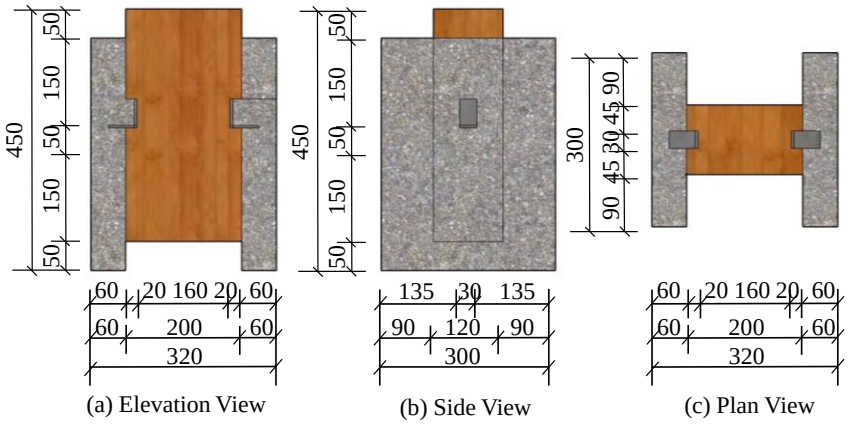

Fig. 1. Dimensions of the timber–concrete composite reversed cyclic specimens (in mm)

Taking into account the Eurocode 5 (2004) and the study of He *et al*. (2016), the dimensions of the timber and concrete blocks were 200 mm × 120 mm × 400 mm and 60 mm × 300 mm × 400 mm, respectively. The dimensions of the specimens subjected to reversed cyclic load are shown in Fig. 1.

The TCC specimens were manufactured in three steps. First, two grooves were made on the left and right sides of the timber block. Second, one angle steel connector was spread with aqueous polyurethane adhesive and then glued in the bottom surface of groove on each side of the timber block. Finally, the concrete was poured into pre-assembled moulds and after 28 d, the moulds were disassembled. The manufacturing of the TCC specimens is shown in Fig. 2.

(a) Groove in timber (b) Connector glued in groove (c) Pouring of concrete

Fig. 2. Manufacturing of the TCC specimens

Material Properties

The timber blocks in this study were made from Xing'an larch, grown in the forest of the Great Khingan Mountains of China. The timber was tested according to GB/T standard 50708 (2012), as shown in Fig. 3a. The compressive strength of the timber was 44.8 MPa, and the experimental mean modulus of elasticity (MOE) of the timber was 13.84 GPa at a moisture content of 11.81%.

Normal–weight concrete with a characteristic compressive strength of 40 MPa was specified for the TCC specimens. The average compressive strength of three 150 mm × 150 mm × 150 mm concrete cubes (after curing for 28 d) was determined to be 45.20 MPa according to Code for design of concrete structures (GB50010-2010), as shown in Fig. 3b.

(a) Compressive test of timber specimens **(b)** Compressive test of concrete cubes

Fig. 3. Tests for the timber and concrete

The angle steel connector consisted of two steel plates with dimensions of 50 mm × 30 mm × 5 mm. The details of the angle steel connector are shown in Fig. 4. The yield strength of the angle steel connectors was 235 MPa, as reported by the manufacturer.

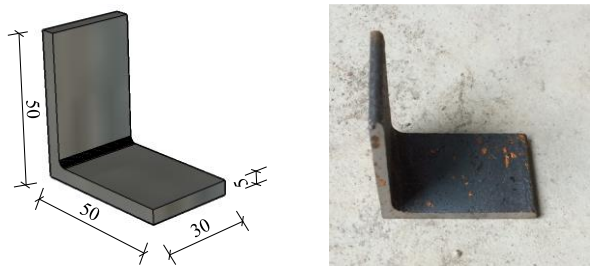

(a) Dimension of connector (b) Photo of connector

Fig. 4. Details of the angle steel connectors

The characteristic properties of the aqueous polyurethane adhesive were provided by the manufacturer. The shear strength was no less than 10 MPa for hardwood and no less than 6 MPa for softwood.

Test Apparatus and Procedure

A specially built apparatus was used for the reversed cyclic test, as shown in Fig. 5. The TCC specimen was placed in the apparatus with the concrete blocks fixed by a concrete fastening device. The timber block of the TCC specimen was fixed to an electrohydraulic servo universal testing machine with a capacity of 250 kN using a junction plate with four high-strength bolt connectors. The push and pull loads were applied to the top and bottom surfaces of the timber block of the TCC specimen.

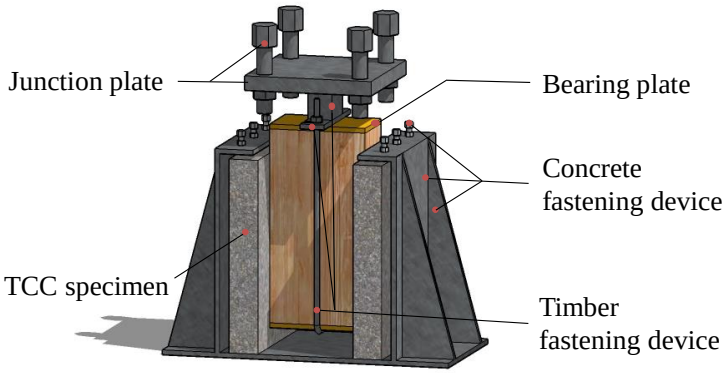

Fig. 5. Testing apparatus for the reversed cyclic tests

The reversed cyclic tests performed on the TCC specimens were conducted according to ISO standard 16670 (2003). The load was applied using a displacement-controlled method with a slip rate of 0.1 mm/s, as shown in Fig. 6. The loading procedure consisted of ten loading steps. From steps 1 to 4, the load was applied once at each step; and from steps 5 to 10, the load was applied three times at each step. The displacement amplitudes for each step are shown in Fig. 6. Based on the mean value of the ultimate displacement in the monotonic tests, calculated according to BS EN standard 26891 (2003), v_u was recorded as the displacement at 0.8 F_{max} in the descending portion of the load–displacement curve (Chen 2016).

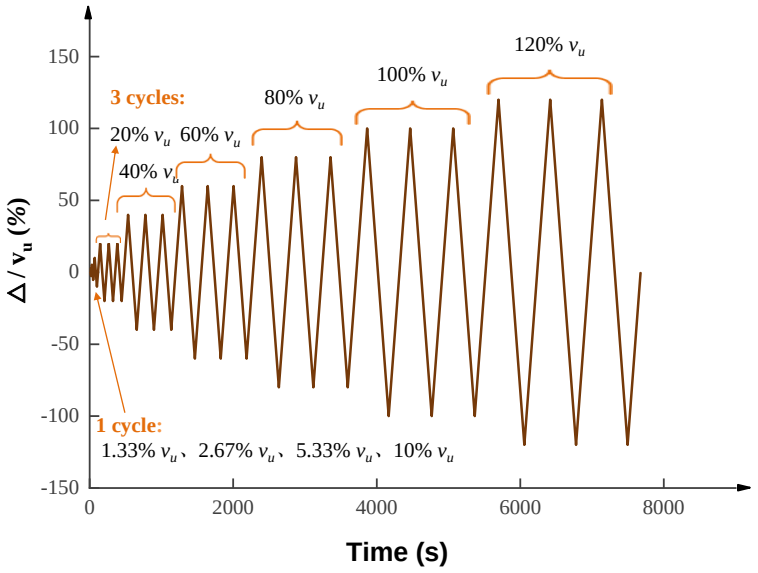

Fig. 6. Loading procedure in the tests according to ISO standard 16670 (2003)

Four displacement gauges were arranged symmetrically on both sides of the specimen to measure the slip between the concrete and the timber. The mean value was recorded as the slip value (*s*). The test apparatus and the arrangement of the displacement gauges are shown in Fig. 7.

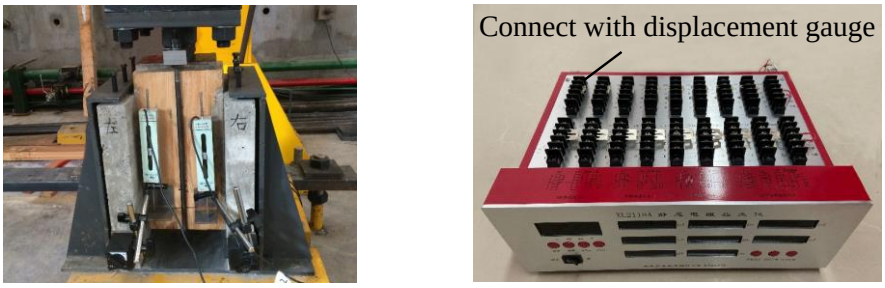

(a) Test apparatus and displacement gauge (b) Measurement apparatus

Fig. 7. Test apparatus and the arrangement of the displacement gauges

RESULTS AND DISCUSSION

Test Phenomenon

During the tests, cracks, deformation of the timber and concrete blocks, and deformation of the angle steel connectors were observed. The failure modes of the six TCC specimens were similar, with the following similarities:

At the initial stage of the positive (push) load, all specimens were in an elastic state. As the controlled displacement (Δ) increased to 0.8 mm, minor fibre compression noise from the timber blocks was heard. As the Δ in the negative (pull) direction reached -0.8 mm, the timber block separated from the concrete block, producing a gap between them. The gap size decreased during the unloading process until the timber and concrete blocks were in contact again during the positive loading process. The gap between the timber and concrete at different stages is shown in Fig. 8a.

After the tests, the failure of the connectors was observed to be the primary factor in terminating the loading procedure. The timber and concrete blocks were separated, and the angle steel connectors failed due to bending deformation (as shown in Fig. 9b). The angle steel connectors failed with one hinge in the vertical limb and another in the horizontal limb. No cracks merged in the timber and concrete blocks. However, there was some fibre compression around the angle steel connectors in the timber block. The concrete blocks after the test as well as the timber fibre compression are shown in Fig 9c and 9d, respectively. For all the specimens, there was no adhesive merged after testing.

(a) Gap between timber and concrete (b) Bending deformation of connector

(c) Spalling of concrete (d) Fibre compression

Fig. 8. The TCC specimen test phenomena

Hysteretic Loops and Skeleton Curves

The specimens had failed when the controlled displacement reached 9 mm. The hysteretic (load–slip) curves are shown in Fig. 9, where the push force is plotted as positive, and the pull force is plotted as negative. As shown in Fig. 9, the hysteretic curves are shuttle-shaped, indicating a pinching effect caused by the slip between the timber and the concrete blocks during the loading process. As the load increased, the slip increased, which was due to the residual deformation during the compression process of the timber and angle connectors. The curves were sharp in the initial stage of unloading and flatten as the controlled displacement (absolute value) decreases.

The skeleton curves for the six specimens are presented in Fig. 10. Residual deformation was observed throughout the test, which indicated that the combination of timber and concrete was flexible to some extent. The TCC specimens failed after some plastic deformation, which indicated that the composite effect of the timber and concrete blocks may involve complex behaviour in terms of the angle steel connector yielding and the local embedding of the wood fibres in compression.

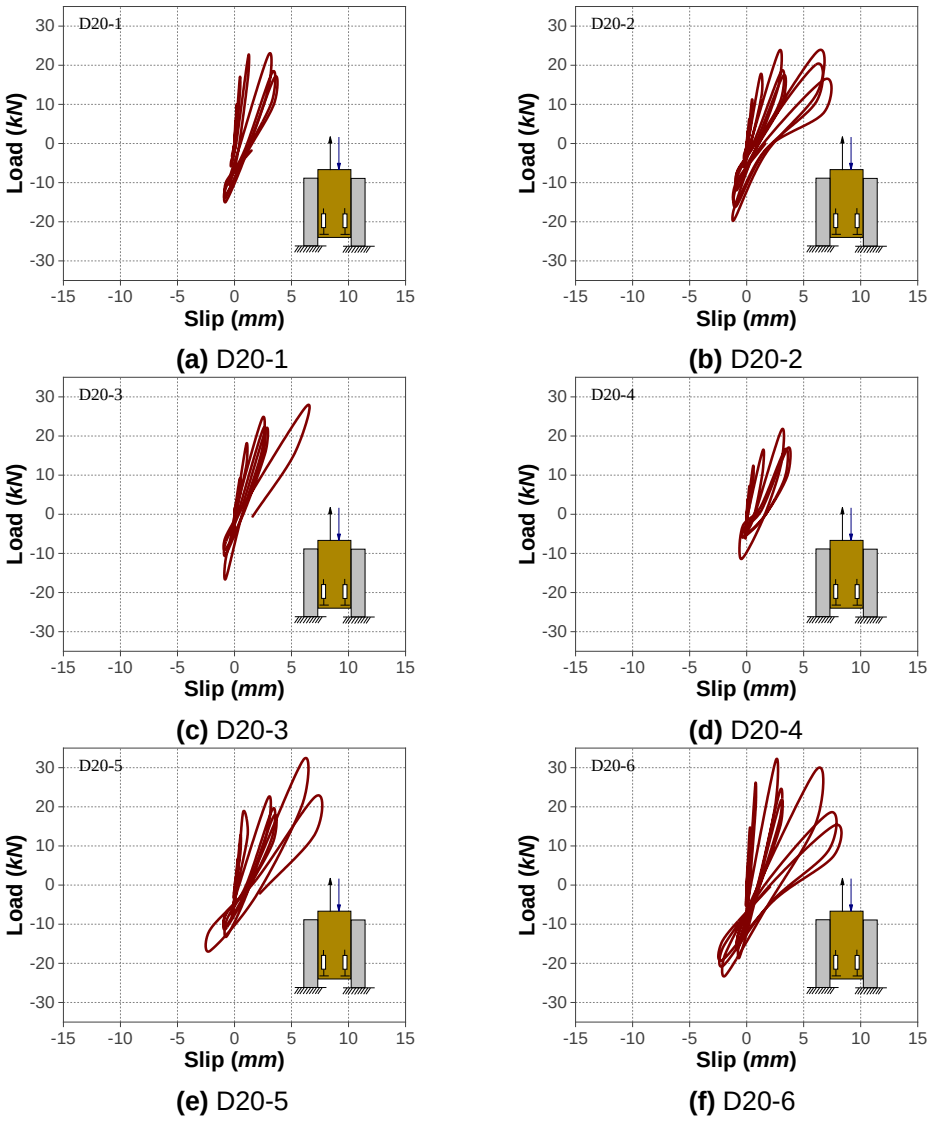

Fig. 9. Hysteretic loops for TCC specimens

As shown in Figs. 9 and 10, the hysteretic curves and skeleton curves were not symmetrical in the positive and negative directions, which may have occurred for two reasons. First, the TCC specimen was pushed and then pulled during the loading procedure. After the positive (push) load was applied, the timber was compressed by the connectors, producing an internal gap between the timber and connector. Thus, the force and corresponding slip in the negative direction were less than the force and corresponding slip in the positive direction. Second, the existing gap between the timber and concrete blocks opened as the timber was pulled and closed as the timber was pushed. Therefore, when the specimen was pulled, a smaller load was required to achieve the specified displacement.

The ultimate shear capacity (F_u), and the corresponding deformability (S_u), slip modulus (K_s), and ductility factor (μ) obtained during the laboratory tests are shown in Table 1. The ultimate shear capacity (F_u) is the maximum load in the hysteretic loop in Fig. 9, and the corresponding deformability (S_u) is the slip corresponding to the maximum load. In addition, the yield deformability (S_y) can also be found as the slip relate to the slope of the curve begin to change. The ductility factor equals the ratio of the ultimate deformability

(S_u) to the yield deformability (S_y). The ductility of the six specimens fluctuated; the ductility factor ranged from 6.00 to 7.78 with a mean value and a coefficient of variation of 6.75 and 0.09, respectively.

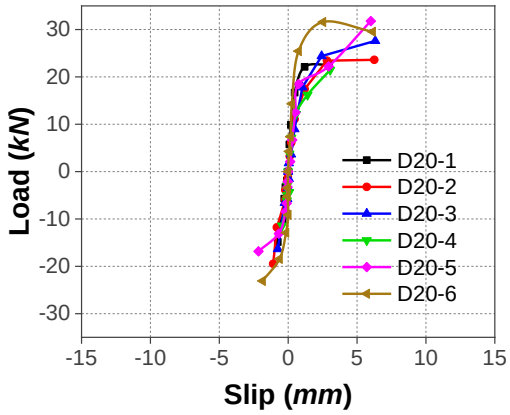

Fig. 10. Skeleton curves for TCC specimens

Table 1. Test Results

No.	F_u (kN)		S_u (mm)		K_s (kN/mm)	μ
	Positive	Negative	Positive	Negative		
D20-1	22.59	-14.87	2.98	-0.76	33.68	7.07
D20-2	23.62	-19.47	6.26	-1.09	15.26	6.00
D20-3	27.61	-16.36	6.32	-0.75	17.28	6.14
D20-4	21.48	-11.41	3.05	-0.44	21.78	6.45
D20-5	31.80	-16.84	6.00	-2.15	23.81	7.10
D20-6	31.60	-22.10	2.53	-1.86	32.27	7.78

Force Mechanism

All specimens were first pushed down and then pulled up. To analyze the force mechanism, three specimen states under reversed cyclic loads were considered.

State I

With the controlled displacement in the range of 0 mm to 0.8 mm, the mean slip of the timber and concrete was 0.80 mm. The TCC specimens were in an elastic state, *i.e.*, the timber, angle steel connectors, and concrete worked cooperatively (as shown in Fig. 12a). The yield load of the TCC specimen can be expressed as Eq. 1,

$$\boldsymbol{F_y = K_s \cdot \delta_i} \quad (1)$$

where F_y is the yield load, K_s is the slip stiffness, and δ_i is the initial slip.

State II

According to the test results, the specimens yielded and became elastic–plastic when the controlled displacement reached 0.8 mm. However, the angle connector did not yield; large plastic deformation was observed in the timber block around the angle connectors due to wood fibre compression. If the stress of the concrete did not exceed its tensile strength, the ductility of the TCC specimen provided by the timber, the strength

provided by the connectors, the deformation of the connectors and timber was restrained by the concrete blocks.

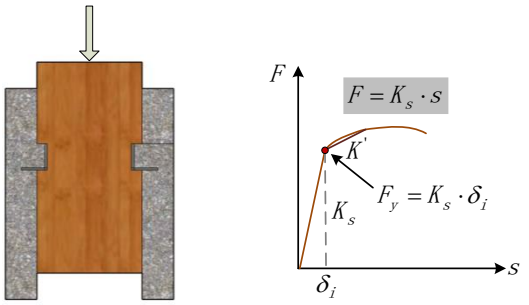

(a) Elastic stage

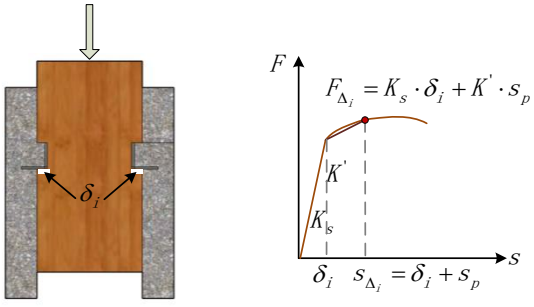

(b) Elastic-plastic stage (downward loading)

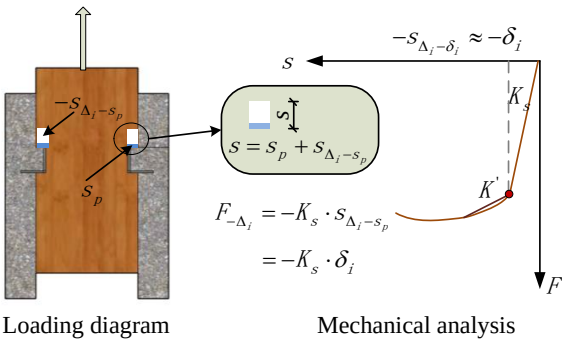

(c) Elastic-plastic stage (upward loading)

Fig. 11. Mechanism of the TCC specimens under cyclic load

As shown in Fig. 11b, the TCC specimen changed from elastic to elastic–plastic under a downward controlled displacement of Δ_i. The specimens exhibited a plastic deformation (s_p) after the initial slip (δ_i). The slip value between the connector and the timber was $\boldsymbol{s_{\Delta_i} = \delta_i + s_p}$, and the load reached $\boldsymbol{F_{\Delta_i}}$. The load of the TCC specimen in the elastic–plastic stage can be expressed as Eq. 2,

$$\boldsymbol{F_{\Delta_i} = K_s \cdot \delta_i + K' \cdot s_p} \quad (2)$$

where $\boldsymbol{F_{\Delta_i}}$ is the load corresponding to the controlled displacement (Δ_i), δ_i is the initial slip, s_p is the plastic deformation corresponding to the controlled displacement Δ_i, and K' is the secant modulus during the elastic-plastic stage.

The TCC specimen behaviour under an upward controlled displacement (-Δ_i) is shown in Fig. 11c. When the controlled displacement was between 0 and -s_p, there was a gap s_p in the vertical direction between the timber and the connector. The timber block moved as a rigid body; the load was equal to the timber gravity plus the friction force between the timber and the concrete. When the controlled displacement was between -s_p and -Δ_i, the load was equivalent to the load under a controlled displacement of $\boldsymbol{\Delta_i - s_p}$, and can be expressed as Eq. 3,

$$\boldsymbol{F_{-\Delta_i} = -F_{\Delta_i - s_p} = -K_s \cdot s_{\Delta_i - s_p} \approx -K_s \cdot \delta_i} \quad (3)$$

where $\boldsymbol{F_{-\Delta_i}}$ is the load corresponding to controlled displacement -Δ_i and $\boldsymbol{F_{\Delta_i - s_p}}$ is the load corresponding to controlled displacement $\boldsymbol{\Delta_i - s_p}$.

The load under the downward displacement (in the positive direction) was larger than the load under the upward displacement (in the negative direction). According to the load–slip curves for the specimens in this study, the controlled displacement Δ_i was approximately equal to the slip between the timber and the concrete (as shown in Fig. 10). According to Eq. 3, $\boldsymbol{s_{\Delta_i - s_p}}$ is approximately equal to δ_i. Thus, the load under the upward controlled displacement -Δ_i only reached the yield strength.

To verify the validity of these equations, the test results for the six specimens were compared with the theoretical results according to these equations. The results indicated good agreement, as shown in Table 2. The $\boldsymbol{F_u}$ represents the ultimate shear capacity, and the $\boldsymbol{F_y}$ represents the yield shear force. The ultimate shear capacity $\boldsymbol{F_u}$ can be found as the maximum force in the hysteretic loops, and the yield force $\boldsymbol{F_y}$ can be found as the point when the slope of the loops begin to change.

Table 2. Comparison of the Theoretical and Test Results

No.	k_s	δ_i	F_u (negative) (kN)		Error	F_y (kN)		Error
			Theoretical Value	Test Value		Theoretical Value	Test Value	
D20-1	33.68	0.47	-15.83	-14.87	0.06	15.83	16.67	-0.05
D20-2	15.26	1.20	-18.31	-19.47	0.06	18.31	17.44	0.05
D20-3	17.28	1.03	-17.80	-16.36	0.09	17.80	17.80	0.00
D20-4	21.78	0.56	-12.20	-11.41	0.07	12.20	12.14	0.00
D20-5	23.81	0.75	-17.86	-16.84	0.06	17.86	18.49	-0.03
D20-6	32.27	0.76	-24.53	-22.10	0.11	24.53	25.46	-0.04

Energy Dissipation Capacity

The energy dissipation curves, according to the first cycle for each loading step, are presented in Fig. 12a. As the controlled displacement increased, the dissipated energy (E) increased to a mean value of approximately 60.70 kJ.

To investigate the energy dissipation of the TCC specimens under reversed cyclic loads, the cumulative dissipated energy in the elastic stage and the elastic–plastic stage were compared, as shown in Fig. 12b. When the controlled displacement reached 0.8 mm, the cumulative dissipated energy ($\sum E$) reached a mean value of 1.69 kJ, representing 3% of the total value. When the specimens were in the elastic stage, the gap between the timber and the concrete was small and unrecoverable; the energy dissipation capacity had not yet

been realized. However, as the TCC specimens moved from the elastic stage to the elastic–plastic stage, the $\sum E$ sharply increased, from less than 2 kJ to 57.23 kJ, reaching 97% of the total value. In this stage, the wood fibre was compressed back and forth by the angle connectors, causing plastic deformation of the wood fibres. The energy dissipation capacity rapidly increased, which indicated that the energy dissipation capacity of the TCC structure was primarily provided by the timber.

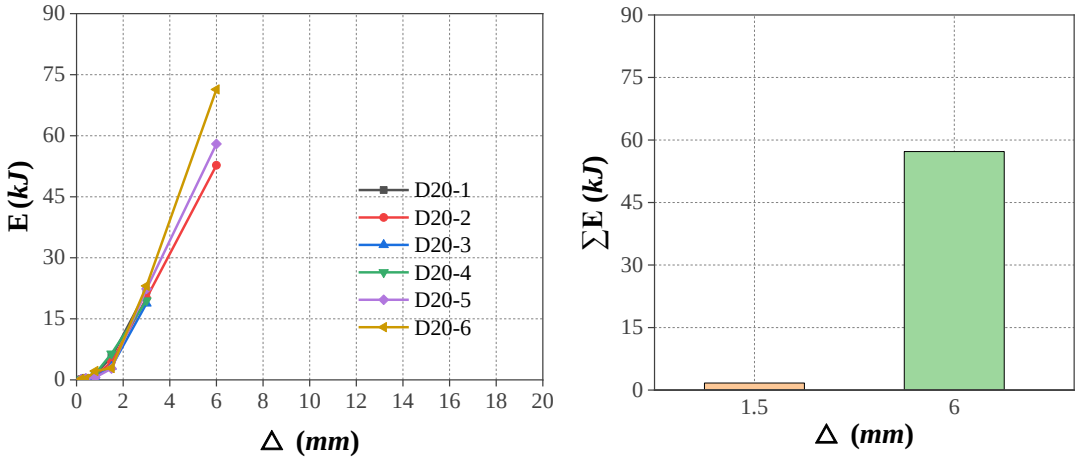

(a) Energy dissipation at every step **(b)** Cumulative energy dissipation6

Fig. 12. Energy dissipation for TCC specimens

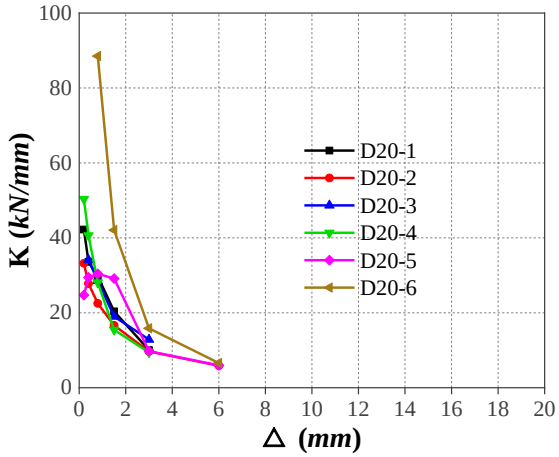

Fig. 13. Stiffness degradation curves

Stiffness Degradation

The stiffness degradation of the angle steel connectors in the TCC specimen was calculated according to Eq. 5,

$$K_i = \frac{|F_i|+|-F_i|}{|\Delta_i|+|-\Delta_i|} \quad (5)$$

where F_i and $-F_i$ are the positive and negative peak loads corresponding to the i^{th} loading displacement, respectively, and $|\Delta_i|$ and $-|\Delta_i|$ are the displacements corresponding to F_i and $-F$, respectively (the results are presented in Fig. 13). As shown in the figure, the stiffness rapidly decreased, which was related to the fibre compression and yielding of the angle

steel connectors. In the later stage, the slopes of the curves tended to flatten. For specimen D20-6, the initial stiffness was higher owing to the good connection between timber and concrete, and it decreased to the same level with other specimens at load step 2.

CONCLUSIONS

This study investigated the angle steel connection used in a timber–concrete composite system. Six reverse-cyclic tests were conducted, and the corresponding failure modes were observed. The salient characteristics of each connection, *i.e.*, stiffness, ductility, and energy dissipation, were calculated from the test results. In addition, the force mechanism of the TCC specimens under a reverse cyclic load was analyzed. Equations were presented for calculating the yield force and the negative force during the same load step. From these results, the following conclusions can be drawn:

1. The failure mode for all specimens was the angle steel connector bending and the local embedding of the wood during compression. The shear capacity of the TCC specimens was primarily provided by the angle steel connectors. The ductility and energy dissipation capacity were primarily provided by the timber and connectors. The deformation of the timber and angle steel connectors was restrained by the concrete.
2. The hysteretic loop had a shuttle shape, which indicated pinching, resulting in degraded strength and stiffness. The pinching effect was caused by the slip between the timber and the concrete. In the elastic–plastic stage, the hysteretic curves were not symmetrical in the positive and negative directions, and the negative force only reached the yield force. This was related to the compression of the wood fibres and the gap between the timber and concrete blocks during manufacturing.
3. The TCC specimens with angle steel connectors performed well in terms of ductility, with a mean ductility factor of 7.78. The cumulative dissipated energy reached 57.23 kJ. Only 3% of the energy was dissipated in the elastic stage; however, 97% of the energy was dissipated in the elastic–plastic stage, primarily due to the plastic deformation of the wood fibres.
4. Based on the force mechanism analysis, the negative force in the elastic–plastic stage was approximately equal to the yield force. The yield force equation was presented, and the theoretical results were verified *via* the experimental results, which indicated good agreement.

ACKNOWLEDGMENTS

This study was supported by the State Forestry Administration Project 948 (Project No. 2014-4-51), the National Natural Science Foundation of China (Grant No. 51478485), the Natural Science Foundation of Hunan Province (Grant No. 2020JJ5618), the Scientific Research Project of Education Department of Hunan Province (19C0169), and the Science Popularization Special Project on the Construction of Innovation-Oriented Provinces (No. 2021ZK4148), all of which are highly appreciated.

REFERENCES CITED

BS EN 1995-1-1:2004. (2004). "Eurocode 5: Design of timber structures–Part 1-1: General–Common rules and rules for buildings," British Standards Institution, London, UK.

BS EN 26891 (1991). "Timber structures. Joints made with mechanical fasteners. General principles for the determination of strength and deformation characteristics," British Standards Institution, London, United Kingdom.

Calil, C., Molina, J. C. (2008). "Numerical evaluation stiffness of connectors "x" in composite specimen of wood and concrete from a cyclical load," *Ciência & Engenharia* 17, 17-26.

Carrero, T., Montaño, J., Santa-María, H., and Guindos, P. (2020). "Static and dynamic performance of direct hybrid connections of cross-laminated timber with steel, concrete and laminated strand lumber composites," *Latin American Journal of Solids and Structures* 17(4), 1-19. DOI: 10.1590/1679-78256106

Chen, W. (2016). *Mechanical Behavior Analysis and Experimental Study on Engineered Timber-Concrete Composite Beam*, Master's Thesis, Central South University of Forestry and Technology, Changsha, China.

Dias, A. M. P. G., Cruz, H. M. P., Lopes, S. M. R., and Kuilen, J. W. v. d. (2010). "Stiffness of dowel-type fasteners in timber-concrete joints," *Structures and Buildings* 163(4), 257-266. DOI: 10.1680/stbu.2010.163.4.257

Frangi, A., Fontana, M., Hugi, E., and Jübstl, R. (2009). "Experimental analysis of cross-laminated timber panels in fire," *Fire Safety Journal* 44(8), 1078-1087. DOI: 10.1016/j.firesaf.2009.07.007

Frangi, A., Knobloch, M., and Fontana, M. (2010). "Fire design of timber-concrete composite slabs with screwed connections," *Journal of Structural Engineering* 136(2), 219-228. DOI: 10.1061/(ASCE)ST.1943-541X.0000101

GB50010-2010 (2010). "Code for design of concrete structures," China Building Industry Press, Beijing, China.

GB/T 50708 (2012). "Technical code of glued laminated timber structures," Standardization Administration of China, Beijing, China.

He, G., Xie, L., Wang, A., Yi, J., Peng, L., Chen, Z., Gustafsson, P. J., and Crocetti, R. (2016). "Shear behavior study on timber-concrete composite structure with bolts," *BioResources* 11(4), 9205-9218. DOI: 10.15376/biores.11.4.9205-9218

He, M., Luo, J., Tao, D., Li, Z., Sun, Y., and He, G. (2020). "Rotational behavior of bolted glulam beam-to-column connections with knee brace," *Engineering Structures* 207, 1-13. DOI: 10.1016/j.engstruct.2020.110251

ISO 16670 (2003). "Timber structures - Joints made with mechanical fasteners - Quasi-static reversed-cyclic test method," Int. Org. Standardization, Geneva, Switzerland.

Isoda, H., and Tesfamariam, S. (2016). "Connections for timber-concrete hybrid building: Experimental and numerical model results," *Journal of Performance of Constructed Facilities* 30(5), 1-12. DOI: 10.1061/(ASCE)CF.1943-5509.0000849

Izzi, M., and Polastri, A. (2019). "Low cycle ductile performance of screws used in timber structures," *Construction and Building Materials* 217, 426-426. DOI: 10.1016/j.conbuildmat.2019.05.087

Kawai, N., Isoda, H., Okabe, M., and Tesfamariam, S. (2016). "Monotonic and reverse-cyclic load experiment for plywood and RC slab diaphragms used in timber-concrete hybrid building," *Structures* 7, 85-99. DOI: 10.1016/j.istruc.2016.05.011

Lamothe, S., Sorelli, L., Blanchet, P., and Galimard, P. (2020). "Engineering ductile notch connections for composite floors made of laminated timber and high or ultra-high performance fiber reinforced concrete," *Engineering Structures* 211, 1-12. DOI: 10.1016/j.engstruct.2020.110415

Leijten, A. J. M., Ruxton, S., Prion, H., and Lam, F. (2006). "Reversed-cyclic behavior of a novel heavy timber tube connection," *Journal of Structural Engineering* 132(8), 1314-1319. DOI: 10.1061/(ASCE)0733-9445(2006)132:8(1314)

Martins, C., Santos, P., Almeida, P., Godinho, L., and Dias, A. (2015). "Acoustic performance of timber and timber-concrete floors," *Construction and Building Materials* 101(Part 1), 684-691. DOI: 10.1016/j.conbuildmat.2015.10.142

Mascia, N. T., and Soriano, J. (2004). "Benefits of timber-concrete composite action in rural bridges," *Materials and Structures* 37(2), 122-128. DOI: 10.1007/BF02486608

Molina, J. C., Calil, C., de Oliveira, D. R., Gomes, N. B. (2019). "Analytical, experimental and numerical study of timber-concrete composite beams for bridges," *Computers and Concrete* 24(2), 103-115. DOI: 10.12989/cac.2019.24.2.103

Rijal, R., Samali, B., Shrestha, R., Crews, K. (2015). "Experimental and analytical study on dynamic performance of timber-concrete composite beams," *Construction and Building Materials* 75, 46-53. DOI: 10.1016/j.conbuildmat.2014.10.020

Rodrigues, J. N., Dias, A. M. P. G., and Providência, P. (2013). "Timber-concrete composite bridges: State-of-the-art review," *BioResources* 8(4), 6630-6649. DOI: 10.15376/biores.8.4.6630-6649

Skinner, J., Bregulla, J., Harris, R., Paine, K., and Walker, P. (2014). "Screw connectors for thin topping, timber-concrete composites," *Materials and Structures* 47(11), 1891-1899. DOI: 10.1617/s11527-013-0158-6

Wacker, J. P., Dias, A. M. P. G., and Hosteng, T. K. (2020). "100-year performance of timber–concrete composite bridges in the United States," *Journal of Bridge Engineering* 25(3), 1-9. DOI: 10.1061/(ASCE)BE.1943-5592.0001513

Xie, L., He, G. J., Wang, A., Gustafsson, P. J., Crocetti, R., Chen, L., Li, L., and Xie, W. (2017). "Shear capacity of stud-groove connector in glulam-concrete composite structure," *BioResources* 12(3), 4690-4706. DOI: 10.15376/biores.12.3.4960-4706

Yang, J.-Q., Smith, S. T., Wang, Z., Feng, P., and Sirach, N. (2020). "Modelling of hysteresis behaviour of moment-resisting timber joints strengthened with FRP composites," *International Journal of Mechanical Sciences* 179, 1-17. DOI: 10.1016/j.ijmecsci.2020.105593

Yeoh, D., Fragiacomo, M., Franceschi, M. D., and Boon, K. H. (2011). "State of the art on timber-concrete composite structures: Literature review," *Journal of Structural Engineering* 137(10), 1085-1095. DOI: 10.1061/(ASCE)ST.1943-541X.0000353

Zhang, L., Zhang, S., and Chui, Y. H. (2021). "Analytical evaluation to the timber-concrete composite beam connected with notched connections," *Engineering Structures* 227, 1-13. DOI: 10.1016/j.engstruct.2020.111466

Zhu, W., Yang, H., Liu, W., Shi, W., Ling, Z., and Tao, H. (2019). "Experimental investigation on innovative connections for timber-concrete composite systems," *Construction and Building Materials* 207, 345-356. DOI: 10.1016/j.conbuildmat.2019.02.079

Article submitted: June 9, 2021; Peer review completed: November 20, 2021; Revised version received and accepted: December 27, 2021; Published: January 5, 2022.
DOI: 10.15376/biores.17.1.1270-1284